Phase-structural and morphological features, dehydrogenation/re-hydrogenation performance and hydrolysis of nanocomposites prepared by ball milling of MgH_2 with germanium

J.A. Adeniran[a], R. Akbarzadeh[a], M. Lototskyy[b], S. Nyallang Nyamsi[b], O.F. Olorundare[c], E.T. Akinlabi[a] and T.C. Jen[a]*

[a] Department of Mechanical Engineering Science, University of Johannesburg, Auckland Park Kingsway Campus, Johannesburg 2006, South Africa

[b] HySA Systems Competence Centre, South African Institute for Advanced Materials Chemistry (SAIAMC), University of the Western Cape, Bellville, South Africa

[c] University of Johannesburg, Auckland Park Kingsway Campus, Johannesburg 2006, South Africa.

Abstract

Ball milling of magnesium hydride with germanium additives in argon for up to 10 hours was shown to result in the formation of nanocomposites of α- and γ-modifications of MgH_2 together with individual Ge phase. During the heating, Ge interacts with MgH_2 to form Mg_2Ge at T>370 °C; the phase transformation overlaps with MgH_2 decomposition and Mg_2Ge phase remains in the material after its re-hydrogenation at T=350 °C and $P(H_2)$~15 bar.

The ball milled Ge-MgH_2 nanocomposites were found to be characterised by an improved hydrogen release via hydrolysis in organic acid solutions as compared to pure MgH_2 prepared and tested at the same conditions. It was found that the composite containing 5 wt% of Ge and ball milled for 5 hours showed the best hydrogen generation performance, with total hydrogen release exceeding 1.55 NL/g (yield close to 100%) in one minute.

*Corresponding author: tjen@uj.ac.za

Keywords: magnesium hydride; germanium; ball milling; phase transformations; hydrolysis

1. Introduction

Studies of hydrogen generation from solid state hydrogen storage materials including light-weight hydrides have gained momentum due to their important features which include relatively low cost,

environmental friendliness and potential for on-board vehicular applications [1,2]. MgH_2 is of a particular interest due to high abundance and low cost of Mg, non-toxicity, as well as high hydrogen storage capacity of MgH_2, 7.66 wt.% H_2 or 0.11 kg(H_2)/L [3-7].

Magnesium hydride and other light weight solid state hydrogen storage materials have been used in mobile fuel cells and light weight military applications. However, major challenge of hydrogen generation by thermal decomposition of these materials (thermolysis) is a slow kinetics of H_2 evolution taking place at high, above 300 °C, temperatures [4-10]. An efficient alternative way for the hydrogen generation is hydrolysis of light metals or hydrides [8-25]. This process takes place at the lower (mostly ambient) temperatures, in neutral, alkaline or acidic medium, and results in high generation of H_2, up to 15% of the weight of the solid material subjected to hydrolysis [9]. In a big number of works dealing with hydrogen generation via hydrolysis, a significant part is focused on the study of composites based on MgH_2 [17-25].

Two major challenges with hydrogen generation by hydrolysis of MgH_2 are the poor reaction kinetics and passivation of the reaction by the $Mg(OH)_2$ by-product [17]. Different methods are being considered to tackle these constrains in order to make the process sustainable. Examples of the proposed methods are: addition of catalysts such as rare earth metals (La, Ce, Pr, Nd and their mixture) [18], carrying out the hydrolysis in the acidic medium [19,20], adding of salts (mostly, chlorides) [17,23,24] to MgH_2 and ball milling of MgH_2 and its composites [21,22,25].

Ball milling improves the reaction kinetics by increasing reaction surface area in the solid products. The ball milling process is associated with fracturing of the crystals in the constituent powders, introducing lattice defects thus increasing number of nucleation sites and facilitating reactivity of the formed products [26], particularly improving the hydrogenation and dehydrogenation kinetics [7]. However, it is evident that no single method could successfully increase hydrogen generation via hydrolysis to a sustainable and scalable level. The ball milling of MgH_2 powders with catalytic additives offers advantages such as synergy between nanostructuring and catalysis resulting in synthesis of new products with improved hydrogen generation potentials.

Germanium has been reported as an effective additive to MgH_2 which lowers the dehydrogenation temperature via thermodynamic destabilization [27,28]. Furthermore, germanium compounds with hydrogen were shown to be effective catalysts of hydrolysis of ammonia borane [16]. Co-milling of MgH_2 with Ge may, therefore, become an efficient way to improve hydrolysis performance of

magnesium hydride. To the best our knowledge, such investigations have not been yet reported in the literature.

In this work, we studied hydrolysis, in aqueous organic acid solutions, of MgH_2 co-milled with Ge. The influence of milling time and Ge/MgH_2 ratio on phase-structural, morphological and H_2 absorption / desorption properties of the Ge-MgH_2 nanocomposites (hereafter referred as GMH), in addition to the change of their performance in the process of hydrogen generation via hydrolysis, were investigated as well.

2. Experimental procedure

2.1 Sample preparation

MgH_2 powder (Rockwood Lithium, 99.8%) and Germanium (99.9%, Across Organic) powders were used as precursors. MgH_2-Ge nanocomposites were obtained by ball milling of the mixture of MgH_2 and Ge powders. The ball milling was carried out using Fritsch F6 planetary mill with tungsten carbide vial and balls at 300 rpm under argon. The ball to powder ratio was of 30:1. The content of germanium in the MgH_2+Ge charge varied between 0 and 20 wt.%, and the milling time – between 1 and 10 hours (see Table 1).

Table1. List of the samples studied in this work

Notation	**Ge additive (wt.%)**	**Milling time (h)**
1GMH	5	1
2GMH	5	2
5GMH0	0	5
5GMH1	5	5
5GMH2	10	5
5GMH3	15	5
5GMH4	20	5
10GMH	5	10

The samples were loaded, unloaded and stored in glove box under purified argon to minimize oxidation during their handling.

2.2 Sample characterization

In addition to hydrogen generation by hydrolysis (see Section 3.2), the gas-phase dehydrogenation and re-hydrogenation properties of the as-milled samples were studied as well. The studies included Thermal Desorption Spectroscopy (TDS; dynamic vacuum, T=20–550 °C, ramp rate 5 °C/min) followed by the re-hydrogenation at T=350 °C and $P(H_2)$~15 bar. The TDS – re-hydrogenation studies were carried out using in-house built Sieverts-type volumetric installation (HySA Systems; see [29] for further details). In addition, for the as-milled samples Thermogravimetric analysis/ Differential scanning calorimetry analysis (TGA/DSC) was carried out, using STA 8000 thermal analyzer (Perkin Elmer); sample weight of 30–50 mg, heating rate of 5 °C/min (T=30–500 °C). Argon was used as the purging gas at a flow rate of 80 ml/min.

X-ray diffraction (XRD) characterization of the samples (as milled and re-hydrogenated) was carried out with Bruker AXS D8 Advance instrument; Cu-Kα radiation, λ_1=1.5406Å, λ_2=1.5444 Å, 2Θ = 10-90º, step of 0.035°. The Rietveld full profile analysis of the as-collected XRD patterns was performed using GSAS software [30]. The standard sample for establishing instrument contribution in peak profile parameters was α-Al_2O_3.

The transmission electron microscopy (TEM) investigation was carried out using JOEL JEM-2100 electron microscope. The samples were suspended in ethanol (99%), sonicated to achieve homogeneity and dropped onto copper grids with holey carbon structures. In addition to taking TEM images, Energy Dispersive Spectroscopy (EDS) and Selective Area Diffraction (SAD) analyses were performed as well.

2.3 Hydrogen generation

Hydrogen generation by hydrolysis was studied using facilities assembled at Department of Mechanical Engineering Science, University of Johannesburg. Fig. 1 shows schematics of the experimental setup. The ball milled GMH powders used for hydrogen generation experiment were placed inside a 2L three-neck borosilicate round-bottom flask. A reaction solution of acetic (*aa*) or citric (*ca*) acid in deionized water (30 to 70 wt.%) was supplied through a funnel connected to the central neck of the flask. The temperature of the reaction was measured by a thermometer inserted in the flask through one of its necks. A hydrogen output pipeline was attached to another neck of the flask. Opening the valve on the funnel marked the commencement of each round of

hydrolysis experiment (start of data logging). Hydrogen gas flew through a tube, a bubbler, a separator (for removal of mist from a gas flow) and a filter (for adsorption of moisture and other impurities) to a flowmeter (Fujikin F100) connected to a data logger. The logged data (50 measurements per a second) were recorded using PC. Each test was carried out two times to confirm reproducibility of the results.

For each experiment, 0.2g of the ball milled sample was used as the hydrogen generation substrate with addition of 50 ml of the reaction solution. The reaction flask was immersed in a water bath maintaining the constant temperature in the range 30 to 60 °C.

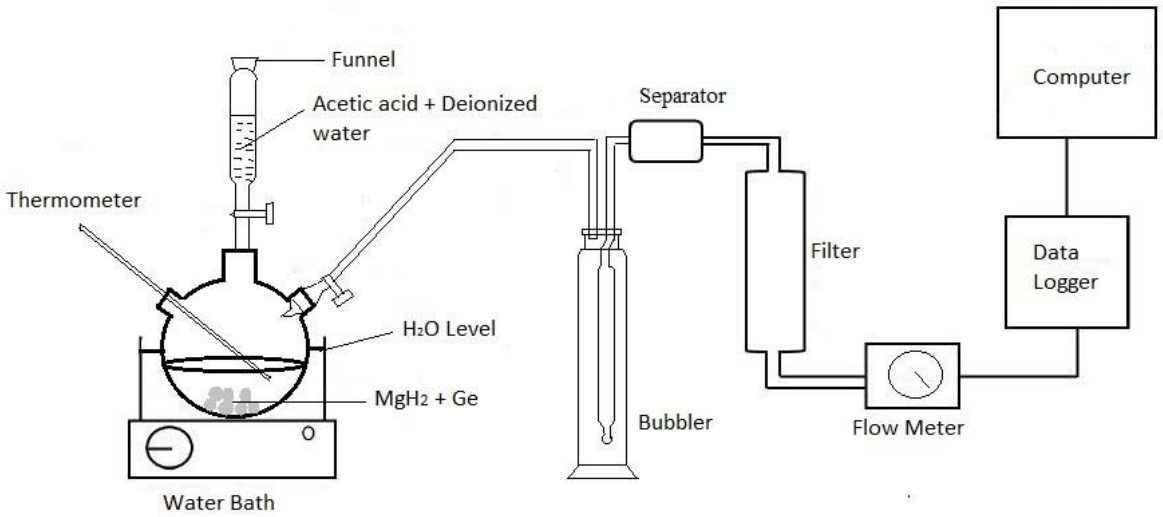

Fig. 1. Experimental setup for hydrogen generation from the Ge+MgH_2 composites

3. Results and discussion

3.1 Samples characterization

3.1.1. Gas-phase dehydrogenation / re-hydrogenation

Fig. 2 presents Derivative thermogravimetry analysis (DTG) (a) and DSC (b) curves of unmodified MgH_2 (5GMH0) and a composite MgH_2–15 wt% Ge (5GMH3) ball milled at the same conditions during 5 hours.

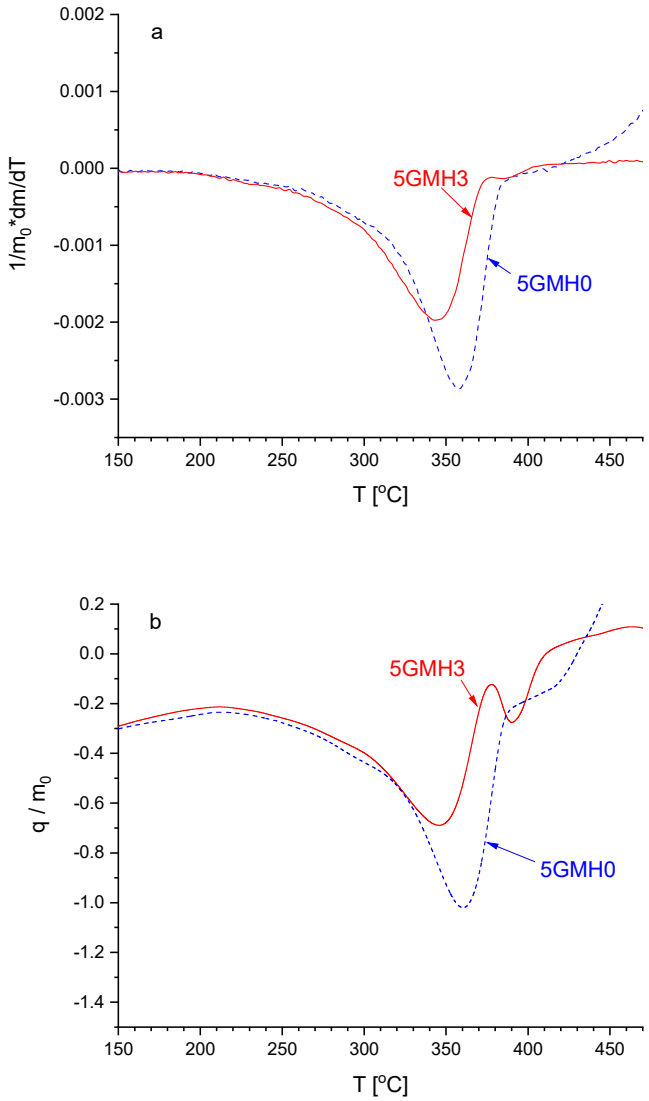

Fig. 2. DTG (a) and DSC (b) plots for the samples 5GMH0 and 5GMH3.

Both samples start to lose weight at T > 200 °C, with a peak at a temperature of 344.5 °C and 357.5 °C for 5GMH3 and 5GMH0, respectively; so introducing Ge results in the decrease of the dehydrogenation peak temperature by 13 °C. The DSC signals follow the DTG ones with a lag of about 3 °C. At T > 400 °C, the unmodified MgH_2 (5GMH0), most probably, undergoes oxidation testified by the weight increase (Fig. 2(a)) and shifting the DSC signal to exo-region (Fig. 2(b)). For the Ge-modified sample (5GMH3) similar performance was observed only at T > 500 °C in a much less pronounced form. We believe that the differences were originated from a less pronounced oxidation of MgH_2+Ge composites as compared to the ball milled MgH_2 rather than

a casual difference of the experimental conditions since each TGA/DSC experiment was repeated 2–3 times.

Additional difference between DSC behaviours of the unmodified and Ge-modified samples (Fig. 2(b)) was in an overlapping of the endo- and exo-effect at T=370–390 °C. The exo-effect can be explained by the interaction of MgH_2 with Ge to form Mg_2Ge whose presence was detected by XRD analysis of both dehydrogenated and re-hydrogenated MgH_2–Ge composites (Section 3.1.2).

Fig. 3(a) shows thermal desorption spectra from the as-milled (#1) and re-hydrogenated (#2) sample 5GMH3. H_2 desorption in vacuum from the as-milled sample (#1) starts at T~300 °C but accelerates only at T>350 °C and finishes at T>500 °C exhibiting two well resolved peaks at T=390 °C and T=435 °C which overlap with a peak at T=414 °C. This behaviour significantly differs from the one observed in the course of the TGA studies (Fig. 2(a)) where continuation of the H_2 evolution was, most probably, suppressed by the sample surface oxidation.

A temporary interruption of the decomposition of MgH_2 in the Ge-doped samples exhibiting an appearance of the high-temperature TDS peaks was not observed for the as-milled non-modified MgH_2 whose TDS pattern was similar to the DTG one for 5GMH0; see Fig. 2(a). The differences increased with the increase of Ge content and disappeared for the TDS of the re-hydrogenated samples all exhibiting one peak at T=390 °C (see curve #2 in Fig. 3(a) as example).

The observed DSC features (Fig. 2(b) and changes of TDS behaviour of the as milled samples upon introducing Ge have their origin in the interaction of Ge with MgH_2 during decomposition of the latter at T~400 °C. The interaction accompanied by the formation of Mg_2Ge phase which inhibits further decomposition of MgH_2 taking place at higher temperatures.

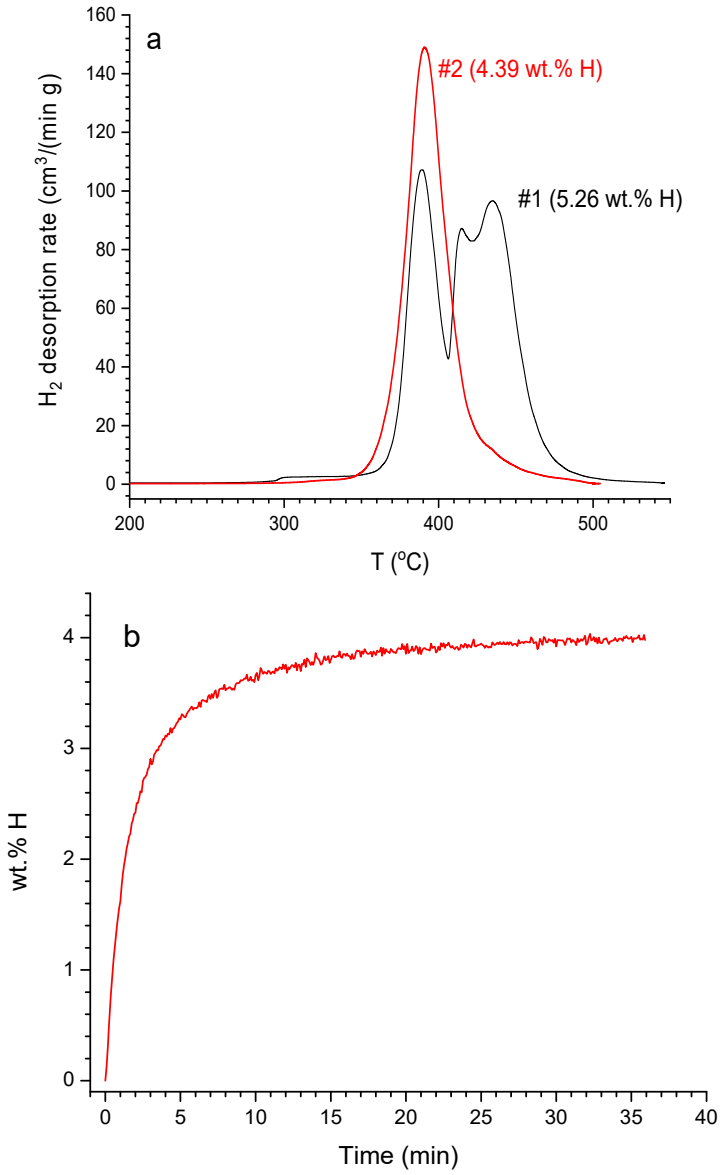

Fig. 3. (a) – TDS of the as-milled (#1) and re-hydrogenated (#2) sample 5GMH3; the values in brackets next to the curve labels show the total amounts of desorbed hydrogen. (b) – re-hydrogenation of the dehydrogenated sample 5GMH3.

The difference of the hydrogen desorption behaviour from the as-milled samples observed in this study from the results reported in refs [27,28] where the introduction of Ge was shown to significantly decrease the H_2 desorption temperature can be explained by the difference of the ball milling conditions when the formation of Mg_2Ge in [27,28] took place already at the stage of ball milling and did not interfere with thermal decomposition of MgH_2. Moreover, as it was reported

in [27], presence of Mg_2Ge (as distinct from Ge) does not change decomposition temperature of MgH_2 that is in a good correspondence with TDS behaviour of the re-hydrogenated samples observed in this work.

Despite very high, above 500 °C, maximum dehydrogenation temperature (Fig. 3(a)) which was shown to result in a deterioration of re-hydrogenation kinetics due to the sintering and recrystallization of Mg and, in turn, slowing down H_2 diffusion through the grown MgH_2 layer [7], the re-hydrogenation of Ge-doped samples during 40–60 min (see Fig 3(b) as example) results in the absorption of more than 4 wt.% H_2, or >80% of hydrogen content in the as-milled samples. In doing so, Ge additives, despite of their interaction with Mg at the higher temperatures, prevent sintering and recrystallization of MgH_2 thus preserving its nanocrystalline morphology.

3.1.2. XRD

Fig. 4 presents as collected XRD patterns of the studied samples. The series shown in Fig. 4(a) presents the data for the samples containing 5 wt.% Ge and milled for different times (1, 2, 5 and 10 hours), and the series in Fig. 4(b) shows the patterns for the samples milled for 5 hours and containing different amounts (0, 5, 10, 15 and 20 wt.%) of Ge additive. The results of Rietveld refinement of the XRD data are summarized in Table 2 (see also Table 1 for the reference to the samples notation).

From the data in Table 2, it can be seen that all the samples contain tetragonal α-modification of MgH_2 as a main constituent; the lattice periods of this phase correspond well to the reference data [31]. The samples also contain minor amounts (5–9 wt.%) of the non-hydrogenated Mg also present in the as-delivered MgH_2 (8.4 wt.%; see Supplementary Information; Fig. S1, Table S1). The ball milling results in a partial transformation of α-MgH_2 into high-pressure orthorhombic γ-modification of magnesium hydride found by a number of researchers in the ball milling experiments [32-34]. Very wide peaks at 2θ around 43° and 63° were assigned to nanocrystalline (5–10 nm) MgO formed due to oxidation of Mg with oxygen adsorbed by a starting powder [33].

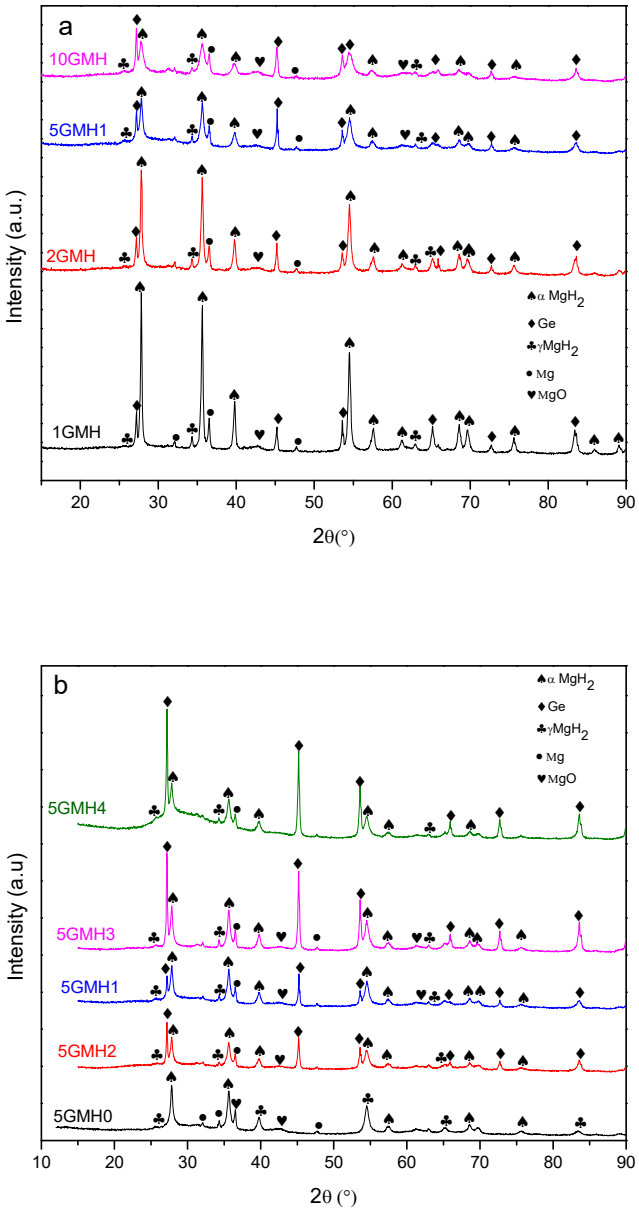

Fig. 4. XRD patterns of the studied samples: effects of ball milling time (a) and precursor ratio (b)

Table 2: Results of Rietveld refinement of the XRD patterns (Fig. 4)

Phase[(a)]	Parameter	Value for the sample:							
		5GMH0	**5GMH1**	**5GMH2**	**5GMH3**	**5GMH4**	**10GMH**	**2GMH**	**1GMH**
α-MgH_2	**Abundance (wt.)**	0.587(-)	0.691(-)	0.621(-)	0.606(-)	0.665(-)	0.589(-)	0.730(-)	0.791(-)
	Crystallite size (nm)	26	29	23	26	24	16	43	75
	***a*(Å)**	4.5201(2)	4.5200(3)	4.5174(4)	4.5172(3)	4.5186(6)	4.5174(4)	4.5174(2)	4.5181(1)
	***c*(Å)**	3.0235(3)	3.0238(3)	3.0224(4)	3.0215(3)	3.0221(6)	3.0227(5)	3.0217(2)	3.0222(1)
γ-MgH_2	**Abundance (wt.)**	0.084(4)	0.065(5)	0.096(6)	0.083(5)	0.072(7)	0.164(5)	0.024(3)	0.078(3)
	Crystallite size (nm)	10	22	17	16	38	8	29	38
	***a*(Å)**	4.52(1)	4.515(8)	4.35(1)	4.243(7)	4.532(6)	4.341(7)	4.481(9)	4.51(-)
	***b*(Å)**	5.43(1)	5.47(1)	5.62(1)	6.11(1)	5.471(8)	5.63(1)	5.64(2)	5.44(-)
	***c*(Å)**	4.95(1)	4.93(1)	5.18(1)	4.95(1)	4.927(9)	5.203(9)	4.90(1)	4.94(-)
Mg	**Abundance (wt.)**	0.073(1)	0.073(2)	0.066(2)	0.058(2)	0.054(3)	0.044(1)	0.075(2)	0.091(2)
	Crystallite size (nm)	170	210	240	630	420	480	100	110
	***a*(Å)**	3.2126(3)	3.2115(5)	3.2105(5)	3.2100(5)	3.2090(7)	3.2110(4)	3.2105(5)	3.2116(4)
	***c*(Å)**	5.211(1)	5.213(1)	5.209(2)	5.210(2)	5.213(2)	5.212(1)	5.208(2)	5.209(1)
MgO	**Abundance (wt.)**	0.256(3)	0.101(4)	0.109(6)	0.084(6)	–	0.140(4)	0.127(6)	0.068(3)
	Crystallite size (nm)	5	10	8	6	–	7	6	10
	***a*(Å)**	4.259(2)	4.235(2)	4.232(4)	4.237(6)	–	4.238(2)	4.231(4)	4.233(3)
Ge	**Abundance (wt.)**	–	0.069(9)	0.109(1)	0.167(1)	0.208(1)	0.062(7)	0.043(1)	0.042(6)
	Crystallite size (nm)	–	84	87	170	140	100	51	81
	***a*(Å)**	–	5.6602(3)	5.6588(2)	5.6583(1)	5.6598(1)	5.6599(2)	5.6589(4)	5.6584(3)
Content of Ge (wt%)		0	5	10	15	20	5	5	5
Milling time (h)		5	5	5	5	5	10	2	1
R_p		0.045	0.047	0.041	0.054	0.060	0.044	0.051	0.054

(a) Reference data [31]:

α-MgH_2: Space Group $P4_2/mnm$ (#136); a = 4.5349 Å, c = 3.0219 Å (ID: 515327);

γ-MgH_2: Space Group: $Pbcn$ (#60); a = 4.4860 Å, b = 5.4024 Å, c = 4.8985 Å (ID: 506717);

Mg: Space Group: $P6_3/mmc$ (#194); a = 3.2125 Å, c = 5.2132 Å (ID: 455030);

MgO: Space Group: $Fm\text{–}3m$ (#225); a = 4.241 Å (ID: 850005);

Ge: Space Group: $Fd\text{–}3m$ (#227) [Origin choice 1]; a = 5.6577 Å (ID: 26034)

For the samples containing germanium, its FCC (diamond structure type) modification was observed in the XRD patterns. The weight abundances of the Ge phase were in a satisfactory correspondence with the initial compositions of MgH_2+Ge mixtures. Furthermore, the lattice period of Ge was in a good agreement with the reference data [31] and did not change with the change of Ge content in the sample and milling time (see Table 2). Similarly, neither MgH_2 (both modifications) nor Mg did show noticeable changes of their lattice periods during co-milling of magnesium hydride with germanium. These observations allow us to conclude that at the ball milling conditions applied in this study the interaction between Ge and Mg (MgH_2), including formation of solid solutions, does not take place. At the same time, the ball milled samples dehydrogenated in vacuum at $T \geq 500$ °C and further re-hydrogenated at $T \sim 350$ °C and $P(H_2) \sim 15$ bar (Fig. 3) showed complete transformation of Ge and part of Mg to CaF_2-type Mg_2Ge intermetallic compound. Presence of Mg_2Ge was observed in both dehydrogenated (see Supplementary Information, Fig. S2) and re-hydrogenated (Fig. 5, Table 3) samples; the latter contains 58.7 wt.% of α-MgH_2 and 2.2 wt.% of Mg that corresponds to ~96% hydrogenation of Mg.

As it can be seen from Fig. 4 and Table 2, the observed changes of the XRD patterns of the studied samples mainly correlate with the milling time. For both modifications of MgH_2 in the ball milled samples, the increase of the milling time results in the decrease of intensities and broadening of the corresponding peaks caused by the reduction of the crystallite size: from 75 to 16 nm for α-MgH_2 (see also Fig. 6(a)) and from 38 to 8 nm for γ-MgH_2 when the milling time increases from 1 to 10 hours. Longer duration of the milling also results in the increase of the abundance of γ-MgH_2 (Fig. 6(b)). Introducing Ge in the charge does not significantly change the observed tendencies as compared to MgH_2 ball milled without additives (Fig. 6). However, for the samples containing Ge, γ-MgH_2 appears already after 1 hour-long milling while for MgH_2 without Ge additive it was observed only for the samples ball milled for 2 and more hours (Fig. 6(b)).

The crystallite size of the Ge phase (samples containing 5 wt.% Ge; see Table 2 and Fig. 6(a)) first decreases from 81 to 51 nm when increasing milling time from 1 to 2 hours. Further increase of the milling time results in a gradual increase of the crystallite size approaching 100 nm for the sample ball milled for 10 hours. This observation allows us to assume that during long milling recrystallization of Ge takes place.

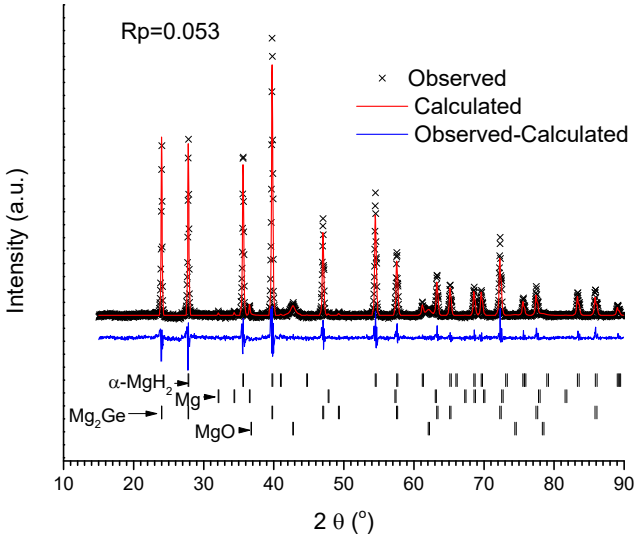

Fig. 5. Refined XRD pattern of the re-hydrogenated sample 5GMH3 (Fig.3(b)).

Table 3. Results of Rietveld refinement of the re-hydrogenated sample 5GMH3 (Fig. 4).

Phase	**Parameter**	**Value**
α-MgH_2	**Abundance (wt.)**	0.587(-)
	Crystallite size (nm)	170
	***a*(Å)**	4.5173(1)
	***c*(Å)**	3.0215(1)
Mg	**Abundance (wt.)**	0.022(2)
	Crystallite size (nm)	350
	***a*(Å)**	3.208(1)
	***c*(Å)**	5.201(4)
MgO	**Abundance (wt.)**	0.112(6)
	Crystallite size (nm)	16
	***a*(Å)**	4.220(2)
Mg_2Ge[a]	**Abundance (wt.)**	0.279(2)
	Crystallite size (nm)	250
	***a*(Å)**	6.3911(1)

[a] – Mg_2Ge: Space Group: *F*m–3m (#225), Structure Type: CaF_2, *a*=6.38 Å ([31], ID: 34076)

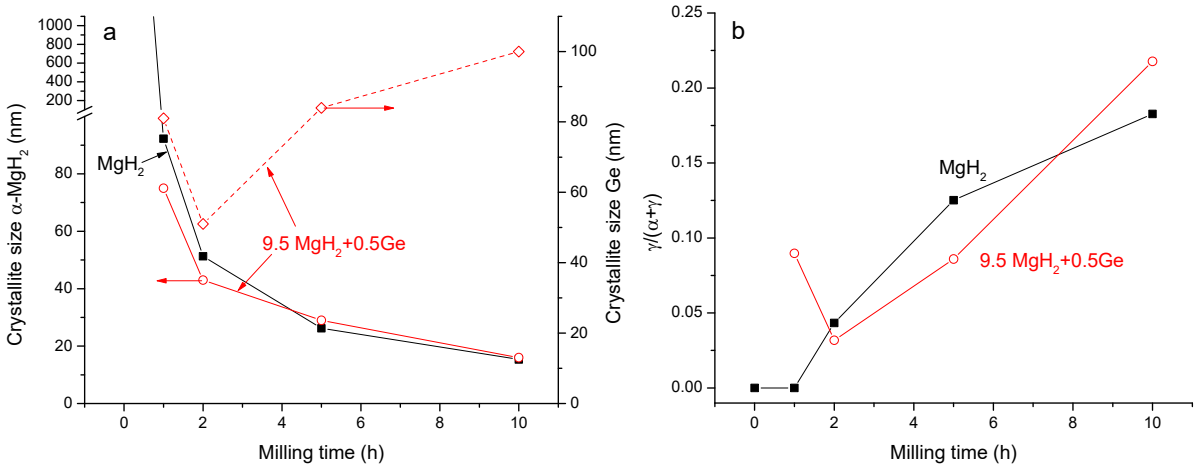

Fig. 6. Dependencies of α-MgH_2 and Ge crystallite sizes (a) and weight fraction of γ-modification in MgH_2 (b) on the milling time of MgH_2 without (black symbols / lines) and with Ge additive (red symbols / lines; curve labels denote sample composition in weight fractions).

The increase of Ge content in the sample from 10 to 15 wt.% results in a significant increase (from 87 to 170 nm) of the crystallite size of Ge in the sample ball milled for 5 hours. Similar value (140 nm) was observed for the sample containing 20 wt.% Ge milled at the same conditions (see Table 2).

3.1.4. TEM

TEM images of the studied ball milled samples MgH_2+Ge (see Fig. 7 and Fig. S3 in the Supplementary information; left) show inclusions of Ge (dark grey; up to 100 nm in the size) uniformly distributed in the bigger particles of magnesium hydride (light grey). All the images show a large spread in particle size of MgH_2 ranging from 100 nm to a few microns.

The SAD patterns of the studied samples (Fig. 7 and Fig. S3 in the Supplementary information; right) show that all the constituent phases are well-crystallized mostly exhibiting diffraction rings formed by well pronounced spots. The positions of the rings (Fig. 7, right) are in a satisfactory correspondence with the XRD data (Table 2).

Fig. 8(a) shows TEM image of the sample 5GMH2, where distances between clearly visible lattice fringes were measured. The distances of 0.251 and 0.31 nm correspond well to (101) and (110)

interplanar distances for tetragonal α-MgH_2 while the distance of 0.55 nm is in a good correspondence with *d*-spacing for (010) planes for γ-MgH_2 [35].

EDS studies (see Fig. 8(b) as example) confirmed the elemental compositions of the studied samples to be in a good correspondence with MgH_2:Ge ratio in the starting charge, as well as weight abundances of the components retrieved from the XRD data.

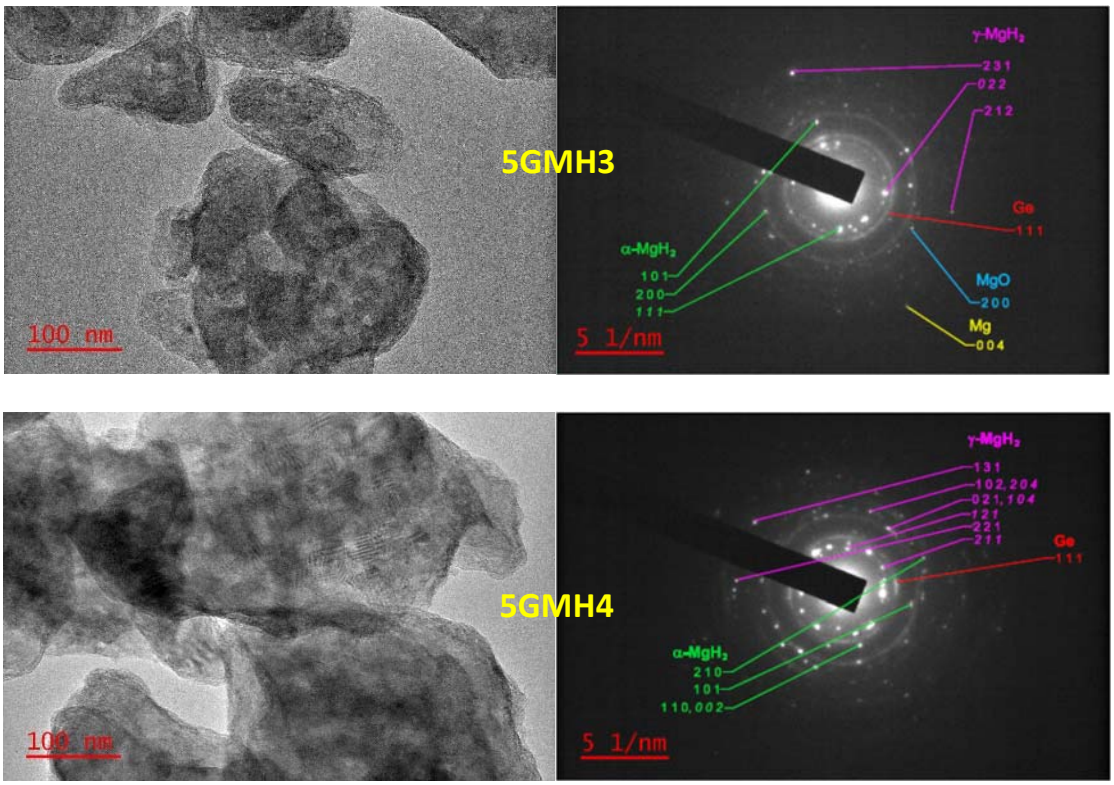

Fig. 7. TEM images (left) and indexed SAD patterns (right) for the samples 5GMH3 (15 wt.% Ge) and 5GMH4 (20 wt.% Ge). Miller indexes on the SAD patterns shown in italic correspond to the second order reflections

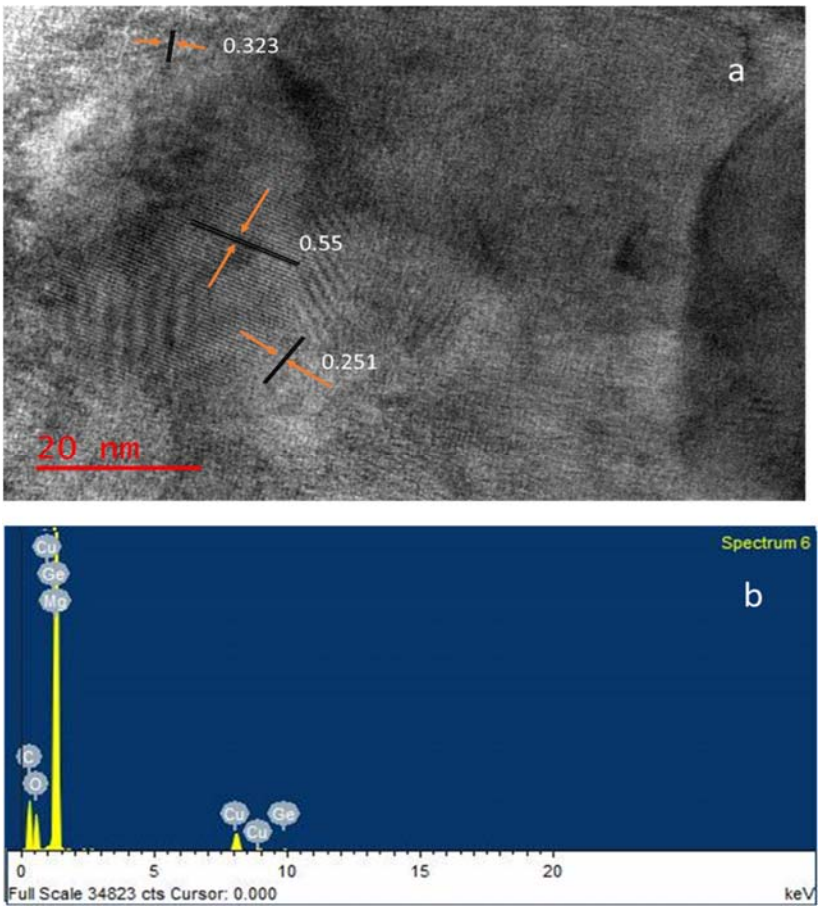

Fig. 8. TEM image (a) and EDS spectrum (b) of the sample MgH_2 + 10 wt.% Ge ball milled for 5 hours (5GMH2). The peaks of C and Cu in (b) correspond to the contribution of copper grid with holey carbon structure holding the sample.

3.2. Hydrolysis of the studied samples

Results of the hydrolysis experiments are summarized in Table 4. The last column of the table specifies the ratio of the total amount of H_2 (integrated flow rate; the column before last) released during 1 minute since the start of hydrolysis reaction to the theoretical amounts of the generated H_2 calculated from the amount of the sample taken for the hydrolysis experiments (0.2 g), content of MgH_2 in the sample (Table 1; assuming no interaction of Ge with the acid solution) and the equation of the hydrolysis reaction:

$$MgH_2 + 2\ H_2O \rightarrow Mg(OH)_2 + 2\ H_2; \qquad (1a)$$

or, taking into account acidic medium applied in the experiments,

$MgH_2 + 2\ H^+ \rightarrow Mg^{2+} + 2\ H_2$; (1b)

Table 4. Summary of the hydrolysis experiments.

#	Sample characteristics			Hydrolysis conditions			H_2 generation (t=1 min)	
	Notation	**Content of Ge (wt.%)**	**Milling time (h)**	**Acid**	***C* (wt.%)**	***T* (°C)**	**Release (NL)**	**Yield (%)[(a)]**
1	5GMH0	0	5	*aa*	50	30	0.2278	66.9%
2	1GMH	5	1	*ca*	30		0.3110	100.9%
3				*aa*			0.3003	97.8%
4					40		0.2780	83.4%
5					60		0.2158	97.7%
6					70		0.2965	96.1%
7	2GMH		2		50		0.3190	104.4%
8	5GMH1		5				0.3225	103.5%
9	10GMH		10				0.2789	89.1%
10	5GMH2	10	5				0.2818	97.5%
11	5GMH3	15					0.2774	104.8%
12	5GMH4	20					0.2588	102.8%
13						40	0.2496	101.2%
14						50	0.2591	102.8%

[(a)] Values above 100% appeared because of the measurement errors

Typical kinetic curves of the reaction (time dependencies of flow rate of released H_2) are presented in Fig. 9. All the data show that the reaction proceeds very fast and virtually completes in 1–2 minutes, in a good correspondence with the reference data on hydrolysis of MgH_2 in aqueous organic acid solutions [19].

As it can be seen from Fig. 9 and Table 4 (experiment / curve #1), the ball milled unmodified MgH_2 exhibits the slowest kinetics of H_2 evolution, with approximately constant reaction rate during the first 10 seconds of the reaction gradually decreasing thereafter. Such behaviour can be explained by the formation of $Mg(OH)_2$ which cannot be completely dissolved in the acid in a short time and thus blocks the surface of remaining MgH_2 preventing hydrolysis according to Reaction (1a). Even in the concentrated (50 wt.%) acetic acid, the total amount of H_2 released in 1 minute was below 70% of the theoretical one.

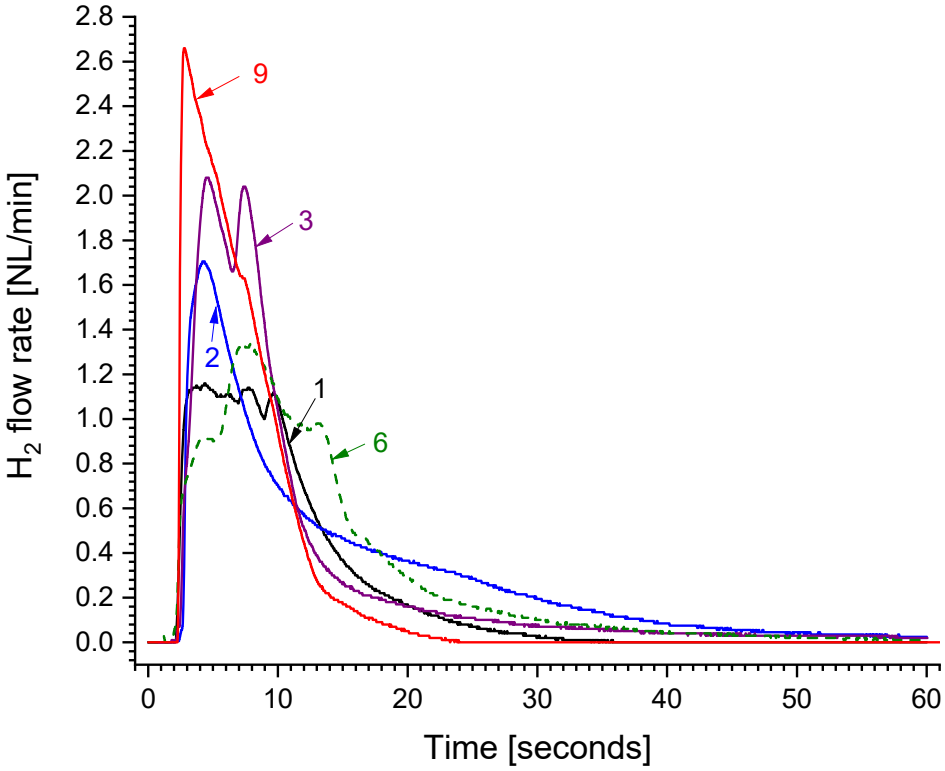

Fig. 9. Hydrolysis of MgH_2–Ge composites. Curve numbers correspond to the numbers of experiments specified in first column of Table 4.

Introduction of 5–20 wt.% Ge in the composite significantly improves hydrolysis performance of MgH_2 when >80% H_2 yield is observed after less than 1 minute. At the optimal hydrolysis conditions (30–50 wt.% of acetic or citric acid at T=30 °C) the yield approaches 100% (see Table 4). The H_2 generation of ~1.56 NL/g, was achieved for the composites containing 5 wt.% Ge; the increase of Ge content to 20 wt.% results in the lowering of the amount of the generated H_2 to 1.26 NL/g.

The reaction rates (Fig. 9; curves 2, 3, 9) significantly exceed the one for the unmodified MgH_2 (curve 1). Interesting feature of hydrolysis of the MgH_2–Ge composites in 30% acetic acid at *T*=30 °C is in a presence of two stages of H_2 evolution with maximum rates observed in around 4.5 an 7.5 seconds after start of the reaction (see Fig. 9, curve 2 as an example).

The increase of ball milling time from 1 to 10 hours does not significantly change the kinetics of hydrolysis of MgH_2–Ge (5 wt.%) composite (50 wt.% *aa*; T=30 °C). However, for the sample 10GMH ball milled for 10 hours (#9), a noticeable decrease of H_2 yield was observed despite of the fastest reaction kinetics at the beginning. This sample was also characterised by the highest abundance of MgO observed in the course of XRD studies of ball milled MgH_2 – Ge composites (see Table 2; 10GMH). We note that the low H_2 yield from unmodified ball milled MgH_2 (#1) can also have its origin in the presence of high amount of MgO in this sample (Table 2; 5GMH0). However, the unmodified MgH_2 also exhibited 1.5–2.5 slower H_2 generation rates than MgH_2–Ge composites (Fig. 9).

As it can be seen from Fig. 9 and Table 4, both citric (curve 2) and acetic (curve 3) acid at the concentration of 30% and T=30 °C provide almost complete hydrolysis of MgH_2 – 5 wt.% Ge composite in ~1 minute. The H_2 evolution kinetics is, however, faster for the acetic acid. Most probably, the difference is related to the different pKa values of the studied acids related to their reactivity with the substrate [36-38].

The increase of the concentration of acetic acid from 30 to 60 wt.% results in the improvement of the reaction kinetics, in agreement with the literature data [38-40]. Further increase of the *aa* concentration to 70 wt.% results in slowing the hydrolysis down (see Fig. 9, curve 6), but the reaction rates remain fast resulting in the H_2 release above 95% of the theoretical amount in one minute.

The increase of reaction temperature from 30 to 50 °C does not significantly change the reaction performance. At all the temperatures (sample 5GMH4, 50 wt.% *aa*) the yield of H_2 achieved in one minute was close to 100% (Table 4; ##12–14).

The improvements of hydrolysis reaction by the addition of Ge can be explained by the incorporation of Ge into MgH_2 matrix during ball milling testified by TEM studies in this work (section 3.1.4). The formation of heterogeneous nanostructures in the materials due to ball milling results in the increase of reaction surface area, increase of the number of nucleation centres and creation of micro-galvanic cells between well-distributed Mg and the foreign metal particles (Ge in our case) [40-47]. Additional improvements may be due to high reactivity of MgH_2–Ge interface in the ball milled composites which easily undergo phase transformation $MgH_2 + Ge \rightarrow Mg_2Ge$

which, as it was shown in this work, takes place at a moderate heating and overlaps with thermal decomposition of MgH_2.

Conclusions:

This study explored MgH_2–Ge nanocomposites prepared by high-energy ball milling of MgH_2 with 5–20 wt.% Ge in argon atmosphere. It was shown that under ball milling conditions (300 rpm, 30:1 balls-to-powder weight ratio) Ge does not interact with magnesium hydride. The interaction, however, takes place during the heating of the ball milled product to T>370 °C and overlaps with thermal decomposition of MgH_2 to form Mg and Mg_2Ge. The latter phase remains unchanged after re-hydrogenation at T=350 °C and $P(H_2)$~15 bar.

For the first time, we showed that the ball milled Ge-MgH_2 nanocomposites are characterised by excellent kinetics of hydrogen release via hydrolysis in organic acid solutions, with total hydrogen release exceeding 1.55 NL/g (yield close to 100%) in one minute.

Hydrolysis of the MgH_2–Ge nanocomposites can become a promising method for onsite hydrogen generation in a number of hydrogen fuel cell applications.

Acknowledgements

This work was supported by funding from the University of Johannesburg and funding from TIA grant. Authors equally appreciate the National Research Foundation (NRF) South Africa for funding the study of the first author. Dr. Akbarzadeh would like to acknowledge the financial support for her Postdoctoral Fellowship from Global Excellence Stature (GES) program.

ML and SNN acknowledge financial support from the Department of Science and Technology / DST of South Africa, within Hydrogen South Africa (HySA) Key Programme KP6 – Metal Hydride Materials and Technologies. ML also acknowledges NRF support; incentive funding grant number 109092. Authors would also like to acknowledge the helpful suggestions of Dr. Fono-Tamo at the pre-planning stage of the ball milling experiment.

References

1. Hosseini SE, Wahid MA. Hydrogen production from renewable and sustainable energy resources: promising green energy carrier for clean development, Renew Sustain Energy Rev 2016; 57: 850-66.
2. Liu W, Webb C, MacA Gray E, Review of hydrogen storage in AB_3 alloys targeting stationary fuel cell applications, Int J Hydrogen Energy 2016; 41(5): 3485-507.
3. Pollock TM. Weight loss with magnesium alloys, Science 2010; 328(5981): 986-7.
4. Webb CJ. A review of catalyst-enhanced magnesium hydride as a hydrogen storage material, J Phys Chem Solids 2015; 84: 96-106.
5. Schlapbach L, Züttel A. Hydrogen-storage materials for mobile applications, Nature 2001; 414(6861): 353-8.
6. Schlapbach L. Technology: Hydrogen-fuelled vehicles, Nature 2009; 460(7257): 809-11.
7. Yartys VA, Lototskyy MV, Akiba E, Albert R, Antonov VE, Ares JR, et al, Magnesium based materials for hydrogen based energy storage: past, present and future, Int J Hydrogen Energy 2019; in press. doi: 10.1016/j.ijhydene.2018.12.212.
8. Jain IP, Jain P, Jain A. Novel hydrogen storage materials: A review of lightweight complex hydrides, J Alloys Compds 2010; 503: 303-39.
9. Tarasov BP, Burnasheva VV, Lototsky MV, Yartys VA. Hydrogen storage methods and opportunities of use of metal hydrides, Int Sci J Altern Energy Ecol (ISJAEE) 2005; 12(32): 14-37.
10. Durbin DJ, Malardier-Jugroot C. Review of hydrogen storage techniques for on board vehicle applications, Int J Hydrogen Energy 2013; 38: 14595-617.
11. Haertling C., Hanrahan Jr RJ, Smith R. A literature review of reactions and kinetics of lithium hydride hydrolysis, J Nucl Mater 2006; 349: 195-233.
12. Jiang HL, Xu Q. Catalytic hydrolysis of ammonia borane for chemical hydrogen storage, Catal Today 2011; 170: 56-63.
13. Wang CC, Chou YC, Yen CY. Hydrogen Generation from Aluminum and Aluminum Alloys Powder, Procedia Eng 2012; 36: 105-13.
14. Liu BH, Li ZP. A review: Hydrogen generation from borohydride hydrolysis reaction, J Power Sources 2009; 187: 527-34.
15. Chou CC, Chen BH, Lee DJ. Hydrogen storage in a chemical hydride fuel system containing ammonia borane and Ni-Co/r-GO catalyst, Energy Procedia 2014; 61: 142-5.
16. Liu Z, Daia Y, Zheng Z, Huang B. Covalently-terminated germanane GeH and $GeCH_3$ for hydrogen generation from catalytic hydrolysis of ammonia borane under visible light irradiation, Catal. Comm 2019; 118: 46-50.
17. Wang S, Sun LX, Xu F, Jiao CL, Zhang J, Zhou HY, et al. Hydrolysis reaction of ball-milled Mg-metal chlorides composite for hydrogen generation for fuel cells, Int J Hydrogen Energy 2012; 37(8): 6771-5.
18. Ouyang LZ, Xu YJ, Dong HW, Sun LX, Zhu M. Production of hydrogen via hydrolysis of hydrides in Mg–La system, Int J Hydrogen Energy 2009; 34(24): 9671-6.

19. Kushch SD, Kuyunko NS, Nazarov RS, Tarasov BP. Hydrogen-generating compositions based on magnesium, Int J Hydrogen Energy 2011; 36(1): 1321-5.
20. Hiraki T, Hiroi S, Akashi T, Okinaka N, Akiyama T. Chemical equilibrium analysis for hydrolysis of magnesium hydride to generate hydrogen, Int J Hydrogen Energy 2012; 37(17): 12114-9.
21. Ma M, Ouyang L, Liu J, Wang H, Shao H, Zhu M. Air-stable hydrogen generation materials and enhanced hydrolysis performance of MgH_2-$LiNH_2$ composites. J Power Sources 2017; 359: 427-34.
22. Tegel M, Schöne S, Kieback B, Röntzsch L, An efficient hydrolysis of MgH_2-based materials, Int J Hydrogen Energy 2017; 42(4): 2167-76.
23. Grosjean MH, Roué L. Hydrolysis of Mg–salt and MgH_2–salt mixtures prepared by ball milling for hydrogen production, J Alloys Compds 2006; 416: 296-302.
24. Makhaev VD, Petrova LA, Tarasov BP. Hydrolysis of Magnesium Hydride in the Presence of Ammonium Salts, Russ J Inorg Chem 2008; 53(6): 858-60.
25. Hong SH, Kim HJ, Song MY. Rate enhancement of hydrogen generation through the reaction of magnesium hydride with water by MgO addition and ball milling, J Ind Eng Chem 2012; 18: 405-8.
26. Zhang L, Guo X. Microstructural Evolution, Thermal Stability and Microhardness of the Nb–Ti–Si-Based Alloy during Mechanical Alloying. Metals, 2018. 8(6): p. 403.
27. Gennari FC, Castro FJ, Urretavizcaya G, Meyer G. Catalytic effect of Ge on hydrogen desorption from MgH_2. Journal of alloys and compounds 2002. 334(1-2): 277-84.
28. Walker GS, Abbas M, Grant DM, Udeh C. Destabilisation of magnesium hydride by germanium as a new potential multicomponent hydrogen storage system. Chem Comm 2011; 47(28): 8001-3.
29. Nyamsi SN, Yartys V, Lototskyy M. Synthesis of Mg_2FeH_6 assisted by heat treatment of starting materials, Mater Today Proc 2018; 5: 10533-41.
30. Larson AC, Von Dreele RB. GSAS. Report lAUR, 1994: p. 86-748.
31. CRYSTMET database, version 5.8.0, © Toth Information Systems, Inc.
32. Denys RV, Riabov AB, Maehlen JP, Lototsky MV, Solberg JK, Yartys VA. *In situ* synchrotron X-ray diffraction studies of hydrogen desorption and absorption properties of Mg and Mg–Mm–Ni after reactive ball milling in hydrogen, Acta Mater 2009; 57: 3989-4000.
33. Huot J, Liang G, Boily S, Van Neste A, Schulz R. Structural study and hydrogen sorption kinetics of ball-milled magnesium hydride, J Alloys Compds 1999; 293-295: 495-500.
34. Gennari FC, Castro FJ, Urretavizcaya G. Hydrogen desorption behavior from magnesium hydrides synthesized by reactive mechanical alloying, J Alloys Compds 2001; 321: 46-53.
35. Zhou SX, Ran WX, Yang MJ, Wang DX, Chen GQ, Zhang Y, et al. Magnesium hydride of orthorhombic crystal from high-energy ball milling under hydrogen atmosphere. in Advanced Materials Research. 2013. Trans Tech Publ.
36. Huesemann MH, Hausmann TS, Carter BM, Gerschler JJ, Benemann JR, et al. Hydrogen generation through indirect biophotolysis in batch cultures of the

nonheterocystous nitrogen-fixing cyanobacterium Plectonema boryanum. Applied biochemistry and biotechnology, 2010. 162(1): p. 208-220.
37. Lukashev RV, Yakovleva N A, Klyamkin SN, Tarasov BP. Effect of mechanical activation on the reaction of magnesium hydride with water. Russian Journal of Inorganic Chemistry, 2008. 53(3): p. 343-349.
38. Uesugi, H, Sugiyama T, Nakatsugawa I. Production of Hydrogen Storage Material MgH2 and its Applications. Japan: Blocoke Lab. Ltd, 2010.
39. Ouyang L, Ma M, Huang M, Duan R, Wang H, Sun L, et al. Enhanced Hydrogen Generation Properties of MgH2-Based Hydrides by Breaking the Magnesium Hydroxide Passivation Layer. Energies, 2015. 8(5): p. 4237-4252.
40. Fan, MQ, Xu F, Sun LX. Hydrogen generation by hydrolysis reaction of ball-milled Al− Bi alloys. Energy & fuels, 2007. 21(4): p. 2294-2298.
41. Grigorieva TF, Barinova AP, Lyakhov NZ. Mechanosynthesis of nanocomposites. Journal of nanoparticle research, 2003. 5(5-6): p. 439-453.
42. Grosjean MH, Zidoune M, Roué L, Huot JY. Hydrogen production via hydrolysis reaction from ball-milled Mg-based materials. International Journal of Hydrogen Energy, 2006. 31(1): p. 109-119.
43. Fan MQ, Xu F, Sun LX, Zhao JN, Jiang T, Li WX. Hydrolysis of ball milling Al–Bi–hydride and Al–Bi–salt mixture for hydrogen generation. Journal of Alloys and Compounds, 2008. 460(1): p. 125-129.
44. Ouyang LZ, Wen YJ, Xu YJ, Yang XS, Sun LX, Zhu M. The effect of Ni and Al addition on hydrogen generation of Mg3La hydrides via hydrolysis. international journal of hydrogen energy, 2010. 35(15): p. 8161-8165.
45. Huot J, Liang G, Schulz R. Magnesium-based nanocomposites chemical hydrides. Journal of Alloys and Compounds, 2003. 353(1): p. L12-L15.
46. Huot J, Liang G, Boily S, Van Neste A, Schulz R. Structural study and hydrogen sorption kinetics of ball-milled magnesium hydride. Journal of Alloys and Compounds, 1999. 293: p. 495-500.
47. Baláž M. Ball milling of eggshell waste as a green and sustainable approach: A review. Advances in colloid and interface science, 2018. 256: p. 256-275.